

Ultrasound-based Thermal and Elasticity Imaging to Assist Photothermal Cancer Therapy – Preliminary Study

Jignesh Shah, Salavat R. Aglyamov, Konstantin Sokolov, Thomas E. Milner and Stanislav Y. Emelianov
Department of Biomedical Engineering, University of Texas at Austin, Austin, TX 78712, USA
(email: emelian@mail.utexas.edu)

Abstract—Photothermal therapy is a targeted, non-invasive thermal treatment of cancer. Up to 40°C temperature increase is obtained in a small volume of malignant cells by using appropriate photoabsorbers and irradiating the tissue with a continuous wave laser. However, in order to ensure successful outcome of photothermal therapy, the tumor needs to be imaged before therapy, the temperature needs to be monitored during therapy and, finally, the tumor needs to be evaluated for necrosis during and after therapy. We investigated the feasibility of ultrasound imaging to track temperature changes during photothermal therapy and elasticity imaging to monitor tumor necrosis after treatment. The image-guided therapy was demonstrated on tissue mimicking phantoms and ex-vivo animal tissue with gold nanoparticles as photoabsorbers. Ultrasound-based thermal imaging effectively generates temperature maps during therapy while elasticity imaging monitors changes in the mechanical properties of tissue before and after therapy, allowing evaluation of treatment efficacy. Results of our study suggest that ultrasound can be used to guide photothermal therapy.

Keywords—*photothermal therapy; ultrasound; thermal imaging; elasticity imaging; cancer; treatment monitoring*

I. INTRODUCTION

Surgery is the most direct therapeutic intervention for cancer. However, small, poorly defined lesions and tumors embedded in vital organs are difficult to treat surgically. Thermal treatments (e.g., photothermal therapy) induce a temperature increase to kill a small volume of cancerous cells and are an alternative to conventional surgery.

Photothermal therapy (PTT) works on the principle of converting light energy into heat energy leading to tumor necrosis [1-3]. Photoabsorbers such as indocyanine green and metal nanoparticles are used in PTT to cause a selective increase in temperature. However, before PTT, the tumor must be first imaged to identify size and location of the lesion. During the therapeutic procedure, the temperature increase should be remotely monitored to ensure both tumor necrosis and protection of surrounding healthy tissue. Finally, tumor response should be inspected during and after therapy to confirm necrosis and to identify possible resurgence. Therefore, a need exists for an imaging technique that can assist, guide and monitor PTT. We propose to utilize ultrasound-based thermal and elasticity imaging to identify the tumor, to monitor temperature and

tumor necrosis, and to evaluate the outcome of the photothermal therapy.

Various imaging methods including MRI, microwave radiometry, impedance tomography and ultrasound have been used for non-invasive thermal imaging. Using a real-time ultrasound imaging system, the temperature change during PTT can be estimated by measuring thermally induced differential motion of speckle. Indeed, the temperature change causes time shifts in ultrasound echo signals due to both the speed of sound change and thermal expansion of the tissue. However, if the temperature is less than 60°C, the time shifts due to the changes in the speed of sound are much larger compared to the shifts due to thermal expansion effects [4, 5]. Therefore, ultrasound imaging can be used to remotely monitor the temperature changes.

Ultrasound imaging can also be used for elasticity imaging [6]. Elasticity imaging employs the difference in tissue hardness for image contrast. The elastic properties of cancerous tissue and thermally ablated tissue can be vastly different from normal tissue. The basic principle of elasticity imaging is to use an imaging modality (e.g., ultrasound) to track the internal tissue displacement caused by an external or internal force. Multiple ultrasound frames are acquired during tissue deformation, and the induced displacements are measured by block matching or other algorithms [7]. The strain tensor is then estimated from the displacements. Finally, distribution of the tissue Young's modulus can be evaluated from the components of the displacement vector and strain tensor based on mechanical equilibrium equations [8]. Therefore, ultrasound and elasticity imaging can identify the lesion and, given PTT induced changes in mechanical properties, can monitor tumor necrosis.

We report a feasibility test of performing image guided photothermal therapy using ultrasound, thermal and elasticity imaging. A laboratory prototype consisting of an ultrasound imaging system interfaced with continuous wave laser was assembled to perform thermal and elasticity imaging. Results from tissue/tumor mimicking phantoms and ex-vivo tissue samples demonstrate the capability of the system to monitor temperature changes and to perform elasticity imaging during photothermal therapy. In addition, a numerical model is presented to evaluate the effectiveness of PTT in cancerous tissue at different depths. The paper concludes with a discussion of image guided photothermal therapy.

Partial support from the National Institutes of Health under grant EB 004963 is gratefully acknowledged.

II. MATERIAL AND METHODS

A. Experimental set-up

The experimental setup for the image guided PTT is presented in Fig. 1. A continuous wave Nd:YAG laser operating at 532 nm with a fluence of 1 J/cm² was used for photothermal therapy. A 128 element linear array transducer operating at 5 MHz center frequency was used to capture ultrasound data. The direction of the laser beam with respect to the imaging plane is shown in Fig. 1. A baseline ultrasound frame was captured before therapy. Ultrasound frames were acquired every 5 seconds during therapy, which lasted for 3 minutes. Before and after therapy, the elasticity imaging was performed by externally deforming the sample and continuously acquiring echo frames during deformation. The captured data was stored for offline processing.

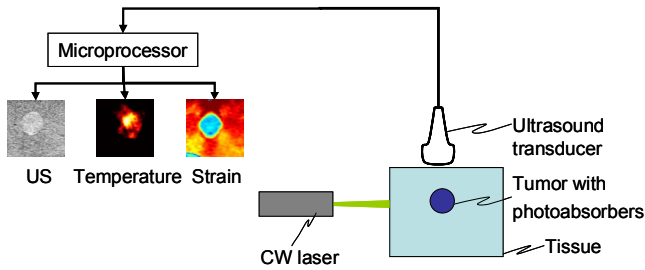


Figure 1. Experimental setup for ultrasound, thermal and elasticity imaging during photothermal therapy.

For both thermal and elasticity imaging, a correlation-based block matching algorithm was employed [7]. A 0.3-mm axial and 0.9-mm lateral kernel was used to obtain an integer estimate of the displacement vector. Interpolation and phase zero-crossings were used to track sub-pixel lateral and axial displacements. Finally, axial strain was computed by using a 1-D difference filter along the axial displacement.

B. Sample preparation

Tissue mimicking phantoms (50 x 50 x 50 mm³) were produced using poly vinyl alcohol (PVA). PVA has modest optical absorption, scatters light similar to tissue and has speed of sound similar to tissue. Specifically, 8% PVA solution was poured into a mold and set to a desired shape by applying two freeze and thaw cycles of 12 hours each. A cylindrical, 7 mm diameter inclusion was embedded in the phantom body to mimic the tumor. Silica particles of 40- μ m diameter were added in the phantom body (0.75%) and the inclusion (1.5%) for acoustic contrast. Gold nanospheres (70-nm diameter) having optical resonance around the 532 nm optical wavelength were added to the inclusion to act as photoabsorbers. Thermal imaging was performed continuously during the 3-minute long photothermal therapy while elasticity imaging was performed before and after therapy.

Tissue studies were performed using two porcine muscle tissue samples (30 x 30 x 15 mm³). The samples were immersed in water for acoustic coupling between the ultrasound transducer and tissue. Sham therapy was performed on the first sample for 3 minutes without adding

nanoparticles. The second tissue sample was injected with nanoparticles (20 μ l of 0.5 \cdot 10¹¹ particles/ml solution) 7 mm away laterally from the site of laser irradiation, and photothermal therapy was carried out to evaluate the effect of nanoparticles on temperature rise. Thermal imaging was performed during both sham therapy and nanoparticle-enhanced therapy.

C. Temperature calibration

A temperature controlled water bath was used to calibrate the temperature response of the tissue mimicking phantom and samples of porcine muscle. To measure the actual temperature, a thermistor was inserted in the center of the sample. First, a baseline echo frame was captured. Then, the temperature of the water bath was increased from 24°C to 38°C, and ultrasound frames were captured for every 1°C temperature increment.

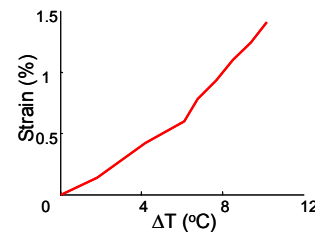


Figure 2a. Temperature calibration for PVA phantom.

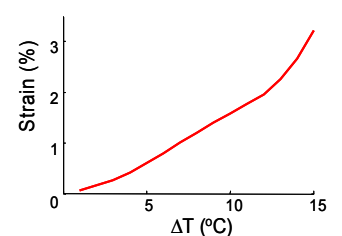


Figure 2b. Temperature calibration for porcine muscle tissue.

The time shifts at each temperature were computed in a 10 mm by 10 mm region near the thermistor using the same cross-correlation based motion tracking method [7]. Strain was then estimated from the corresponding time shifts. We assumed the temperature distribution is spatially homogenous at steady state. Thus, a strain versus temperature dependence was obtained for both the PVA phantom and porcine tissue. A nearly linear relationship was observed between temperature and induced strain (Fig. 2).

D. Modeling

The temperature change during PTT is due to two processes – heat generation by laser excitation and spatial redistribution by diffusion. To describe both processes, a numerical model was developed utilizing the Fourier heat equation:

$$\rho c \frac{\partial T}{\partial t} = \nabla(\lambda \nabla T) + Q_s, \quad (1)$$

where T is temperature (K), ρ is tissue density (kg/m³), c is the specific heat (J/kg/K), λ is the thermal conductivity of the tissue (W/m/K) and Q_s (W/m³) is the external heat term.

Equation (1) was solved using explicit finite difference techniques. Monte Carlo modeling was used to calculate light propagation in a multilayered tissue model. A spherical tumor of 2 mm radius was embedded at depths of 7.5 mm and 15 mm in a homogenous medium measuring 40 mm laterally and 30 mm axially. The optical absorption coefficient (μ_a) of the tumor was varied from 30 cm⁻¹ at

7.5 mm to 900 cm⁻¹ at 15 mm while the scattering coefficient (μ_s) was 100 cm⁻¹. The homogenous tissue had an absorption coefficient of 0.8 cm⁻¹ and scattering coefficient of 10 cm⁻¹. A Gaussian beam with total power of 1 W at 808 nm was chosen to demonstrate the photothermal therapy effect at greater depths in the tissue compared to the 532 nm wavelength used in experimental studies.

III. RESULTS

The results of ultrasound, thermal and strain imaging in the tissue mimicking phantom are presented in Figs. 3a-c. All images cover a 20 mm by 20 mm field of view.

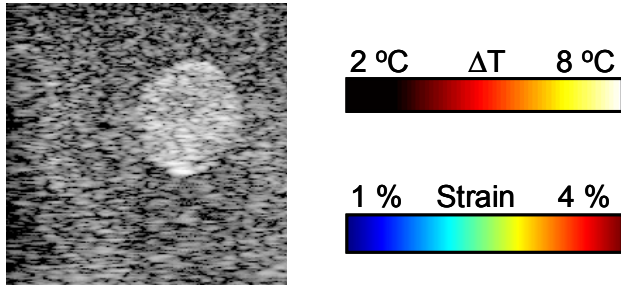


Figure 3a. Ultrasound image of tissue mimicking phantom.

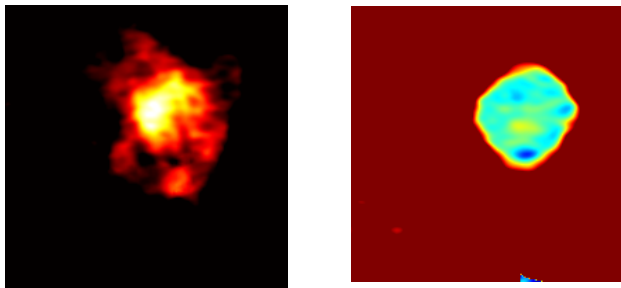


Figure 3b. Thermal image after PTT. Figure 3c. Strain image after PTT.

The grayscale B mode image (Fig. 3a) clearly shows the tumor in an otherwise homogenous phantom. The thermal image (Fig. 3b) shows the temperature map in the phantom immediately after photothermal therapy. The laser radiation was applied on the left side of the phantom. The calibration data (Fig. 2a) was used to convert the accumulated strain into temperature. Progressive increase in temperature during therapy was observed. The inclusion reached a temperature rise of over 7°C at the end of therapy while the surrounding material has a temperature rise of less than 2°C. Furthermore, elasticity imaging was performed at the conclusion of PTT. The harder inclusion having lower strain is visible in the strain image (Fig. 3c). Overall, ultrasound, thermal and elasticity images show excellent co-registration.

Photothermal therapy was also performed using porcine tissue. The ultrasound and thermal images (12 mm by 12 mm field of view) are presented in Figs. 4a-d. The site of laser irradiation and nanoparticle injection is marked on the ultrasound image (Fig. 4b). Temperature increase in the sham treatment was up to 6°C at the end of PTT (Fig. 4c). However, after nanoparticle injection, a temperature increase of over 15°C was observed in the tissue (Fig. 4d). The

approximately 2 mm diameter heated region in the nanoparticle therapy was located 7 mm inside the tissue. In sham therapy, the temperature reached maximum at the surface and gradually decreased with depth.

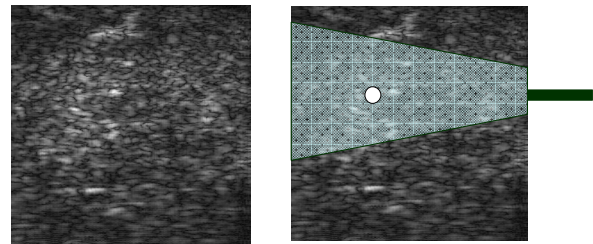


Figure 4a. Ultrasound image of porcine tissue.

Figure 4b. Site of laser irradiation and nanoparticle injection.

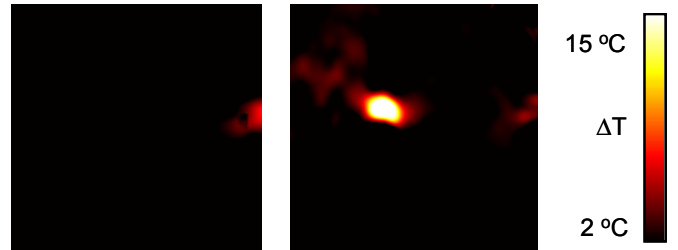


Figure 4c. Thermal image of sham therapy.

Figure 4d. Thermal image of nanoparticle therapy.

The injection of gold nanoparticles in tissue enhanced the photothermal therapy effects. The temperature increase in both sham and nanoparticle therapy experiments along the lateral direction of laser irradiation is presented in Fig. 5. The surface temperature rise in both therapies was similar. However, a highly localized therapeutic zone with a temperature increase of over 15°C was observed in the nanoparticle therapy at the site of photoabsorber injection.

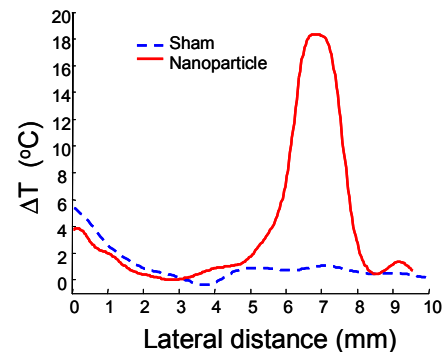


Figure 5. Temperature rise with and without nanoparticles along the laser irradiance plane (Fig. 4a) in a sample of porcine muscle tissue.

A numerical model was constructed to evaluate the effectiveness of photothermal therapy. A laser wavelength of 808 nm was used to induce photothermal effects at varying tumor depths. A temperature increase of over 18°C after 120 seconds of therapy was computed in tissue samples (40 mm by 30 mm field of view) with tumors positioned at 7.5 mm and 15 mm depths (Fig. 6). The surrounding tissue did not exhibit a significant temperature rise (< 6°C). To reach such temperatures in tumor and surrounding tissue with the same

laser fluence and irradiation time, $1.5 \cdot 10^{12}$ particles/ml were injected in the tumor at depth 15 mm (Fig. 6b) compared to $0.5 \cdot 10^{11}$ particles/ml needed at a depth of 7.5 mm (Fig. 6a). Alternatively, a higher fluence or increased irradiation time could be used to target deeper tumors although this could potentially increase non-specific thermal injury of tissue in the near field.

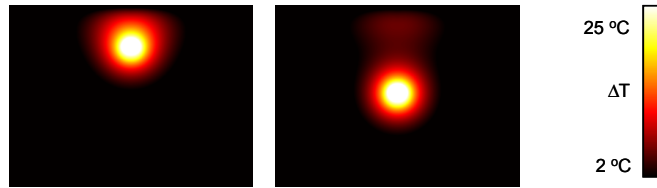


Figure 6a. Therapy of the tumor positioned at 7.5 mm depth.

Figure 6b. Therapy of the tumor positioned at 15 mm depth.

IV. DISCUSSION

By using appropriate photoabsorbers, a selective temperature increase was observed in the tumor with negligible temperature increase in the surrounding body. The images in Fig. 3 illustrate feasibility of using ultrasound, thermal and elasticity imaging to assist photothermal cancer therapy. By continuously monitoring the temperature distribution within the tissue, therapy progression can be tracked to prevent damage of surrounding healthy tissue. Additionally, the change in the mechanical properties of tissue due to thermal damage can be monitored. Elasticity imaging can be performed to evaluate tissue properties. In phantom experiments, the temperature increase was insufficient to cause any variation in the mechanical properties of PVA. In tissue, however, the progression of the tumor necrosis can be assessed by performing elasticity imaging at regular time intervals during and after therapy.

Although laser wavelength and photoabsorber resonance were matched at 532 nm, this optical wavelength is not appropriate for tissue studies – the penetration depth in tissue is less than a few millimeters. However, there exists a near infrared (NIR) optical window of 700–1000 nm [9], where minimal light absorption in tissue leads to greater penetration depths. Various thermal coupling agents such as gold nanorods, gold nanoshells, and indocyanine green have their absorption resonance in this NIR window. Thus by using light in the NIR region with appropriate photoabsorbers, tumors at depths of a few centimeters can be treated by photothermal therapy. Our numerical studies suggest that by using a laser emitting at 808 nm with photoabsorbers resonating at the same wavelength, deep lying tumors can be treated using PTT.

Finally, a photoacoustic imaging can be used both to visualize the tumor and to monitor the therapy. Photoacoustic imaging combines the complementary properties of optics and acoustics to generate high contrast images. The same transducer can be used in ultrasound, photoacoustic and elasticity imaging [6]. The inherent differences in the optical properties of the tumor and the surrounding tissue provide the contrast for photoacoustic imaging. This contrast will be significantly enhanced by the photoabsorbers used for

photothermal therapy. In addition, the pressure of photoacoustic pulse has been shown to be linearly dependent on temperature [10] and can be used to measure temperature. Thus photoacoustic imaging can be utilized to not only image the tumor but also to monitor the temperature change along with ultrasound based methods.

V. CONCLUSION

The results of this study strongly suggest that ultrasound can be used to image and assist photothermal therapy in real time. Experimental results indicate that selective temperature increase due to photothermal therapy can be effectively monitored by ultrasound-based thermal imaging. Furthermore, elasticity imaging performed in conjunction with ultrasound adds a diagnostic tool relevant to treatment efficiency. Additionally, numerical modeling shows by using an appropriate wavelength and photoabsorbers, tumors at a reasonable depth can be treated with photothermal therapy.

ACKNOWLEDGMENT

The authors would like to thank Mr. Larson for his help in making the gold nanoparticles, and Dr. Dunn and Mr. Estrada for providing use of the continuous wave laser.

REFERENCES

- [1] X. Huang, I. H. El-Sayed, W. Qian, and M. A. El-Sayed, "Cancer cell imaging and photothermal therapy in the near-infrared region by using gold nanorods," *Journal of The American Chemical Society*, vol. 128, pp. 2115-20, 2006.
- [2] W. R. Chen, R. L. Adams, S. Heaton, D. T. Dickey, K. E. Bartels, and R. E. Nordquist, "Chromophore-enhanced laser-tumor tissue photothermal interaction using an 808-nm diode laser," *Cancer Letters*, vol. 88, pp. 15-9, 1995.
- [3] C. Loo, A. Lin, L. Hirsch, M. H. Lee, J. Barton, N. Halas, et al., "Nanoshell-enabled photonics-based imaging and therapy of cancer," *Technology in Cancer Research & Treatment*, vol. 3, pp. 33-40, 2004.
- [4] R. Maass-Moreno and C. A. Damianou, "Noninvasive temperature estimation in tissue via ultrasound echo-shifts. Part I. Analytical model," *The Journal of The Acoustical Society of America*, vol. 100, pp. 2514-21, 1996.
- [5] R. Maass-Moreno, C. A. Damianou, and N. T. Sanghvi, "Noninvasive temperature estimation in tissue via ultrasound echo-shifts. Part II. In vitro study," *The Journal of The Acoustical Society of America*, vol. 100, pp. 2522-30, 1996.
- [6] S. Y. Emelianov, S. R. Aglyamov, J. Shah, S. Sethuraman, W. G. Scott, R. Schmitt, et al., "Combined ultrasound, optoacoustic and elasticity imaging," *Proceedings of SPIE*, vol. 5320, pp. 101-112, 2004.
- [7] M.A. Lubinski, S.Y. Emelianov, and M. O'Donnell, "Speckle tracking methods for ultrasonic elasticity imaging using short-time correlation," *IEEE Transactions on Ultrasonics, Ferroelectrics and Frequency Control*, vol. 46, p. 82-96, 1999.
- [8] A. R. Skovoroda, S. Y. Emelianov, and M. O'Donnell, "Tissue elasticity reconstruction based on ultrasonic displacement and strain images," *IEEE Transactions on Ultrasonics, Ferroelectrics and Frequency Control*, vol. 42, pp. 747-765, 1995.
- [9] R. Weissleder, "A clearer vision for in vivo imaging," *Nat Biotechnol*, vol. 19, pp. 316-7, 2001.
- [10] I.V. Larina., K.V. Larin, and R.O. Esenaliev, "Real-time optoacoustic monitoring of temperature in tissues," *Journal of Physics D: Applied Physics*, vol. 38, pp. 2633-2639, 2005.